

## Article

# A Theoretical Study of the N<sub>2</sub> + H<sub>2</sub> Reactive Collisions for High Vibrational and Translational Energies

 Juan de Dios Garrido <sup>1</sup>  and Maikel Yusat Ballester <sup>2,\*</sup> 
<sup>1</sup> Centro Interdisciplinar de Ciências da Natureza, Universidade Federal da Integração Latino-Americana, Foz do Iguaçu 85866-000, PR, Brazil; garrido.jd@gmail.com

<sup>2</sup> Departamento de Física, Universidade Federal de Juiz de Fora, Juiz de Fora 36036-330, MG, Brazil

\* Correspondence: maikel.ballester@uff.edu.br

**Abstract:** High translational temperatures appear in the air inside the shock waves layers created by relatively large meteorites, reentry space vehicles, and hypersonic missiles. Under these conditions, reactions between molecular nitrogen and hydrogen are energetically permitted. In the present work, a quasiclassical trajectories study of the N<sub>2</sub>(*v'*) + H<sub>2</sub>(*v''*) reaction for relative translational energies covering the range of translational energy 20.0 ≤ *E<sub>tr</sub>*/kcalmol<sup>−1</sup> ≤ 120.0 is presented. In the calculations, several values of vibrational quantum numbers *v'* = 0, 4, 6, 8, 10, 12 and *v''* = 4, 6, 8, 10, 12 have been considered. To model the interatomic interactions, a six-dimension global potential energy surface for the ground electronic state of N<sub>2</sub>H<sub>2</sub> was used. The specific initial state reaction cross-sections and rate coefficients are reported. The energy effects produced by the reaction that could influence the shock wave modeling are here considered. An analysis of the possible impact of these processes under the atmospheric composition is also presented.

**Keywords:** molecular collisions; quasiclassical trajectories; atmospheric reactions



**Citation:** Garrido, J.d.D.; Ballester, M.Y. A Theoretical Study of the N<sub>2</sub> + H<sub>2</sub> Reactive Collisions for High Vibrational and Translational Energies. *Atmosphere* **2021**, *12*, 1349. <https://doi.org/10.3390/atmos12101349>

Academic Editor: Luís Pedro Viegas

Received: 13 September 2021

Accepted: 12 October 2021

Published: 15 October 2021

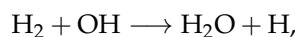
**Publisher's Note:** MDPI stays neutral with regard to jurisdictional claims in published maps and institutional affiliations.



**Copyright:** © 2021 by the authors. Licensee MDPI, Basel, Switzerland. This article is an open access article distributed under the terms and conditions of the Creative Commons Attribution (CC BY) license (<https://creativecommons.org/licenses/by/4.0/>).

## 1. Introduction

Local temperatures in the range of 2000 ≤ *T*/K ≤ 45,000 can be produced in the Earth's atmosphere by the movement of relatively large meteorites, reentry space vehicles, and hypersonic missiles and planes [1–4]. For these temperatures, there is a relatively large number of molecules populating vibrationally excited levels. Then, for such conditions, it is necessary to consider the rate constants of different reactive and nonreactive processes involving vibrationally excited species in works devoted to modeling the movement of the already-mentioned artefacts [2,3,5–7]. In particular, the molecular hydrogen, a minor atmospheric constituent (0.000053 mole percent) [8–10], shows small reactivity for relative low translational energies. For example, their rate constants, in collisions with important atmospheric components such as O and OH for reactions:



have the values  $9 \times 10^{-18}$  and  $6.7 \times 10^{-15} \text{ cm}^3 \text{ s}^{-1} \text{ molecule}^{-1}$  [11,12] at 298 K, respectively. In turn, the atomic hydrogen is involved in the atmospheric reactions:



with rate constant values of  $7.2 \times 10^{-11}$ ,  $7.5 \times 10^{-11}$  and  $2.8 \times 10^{-11} \text{ cm}^3 \text{ s}^{-1} \text{ molecule}^{-1}$ , respectively, at 298 K [11,12], several orders of magnitude higher. It means, that by replacing

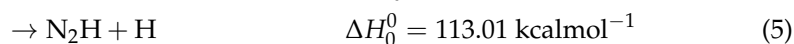
the molecular hydrogen with atomic hydrogen, it is possible produce a high chemical impact in the atmosphere.

The reaction between molecular nitrogen and hydrogen has not been previously considered in technology [13,14] and shock wave [5] simulations, based upon the small value of the rate constant for temperature below 5000 K. Nevertheless, preliminary calculations show relatively high values of the rate coefficients for such a reaction at temperatures above 6000 K [15]. Moreover, the hydrogen atoms produced from title collisions could enter the important reactions (1)–(3) included in the atmospheric ozone cycles [8]. Furthermore, due to the high energy barrier involved, the title reactive collisions could influence the energy balance of the gas. Although an increase in the H<sub>2</sub> dissociation with the vibrational energy is expected, it is not clear how the formation of atomic hydrogen could be affected by the competition with other reactive and nonreactive channels, which also may be stimulated by the participation of vibrationally excited H<sub>2</sub> molecules.

Thus, the major goal of the present work is to report a detailed theoretical study of the reaction between molecular hydrogen and nitrogen at their corresponding ground electronic states, for several initial vibrationally excited combinations. For such a task, the quasiclassical trajectory (QCT) method and the single-valued double many-body expansion (DMBE) potential energy surface for the electronic ground state of H<sub>2</sub>N<sub>2</sub> are used. The paper is organized as follows: Section 2 provides a brief survey of the H<sub>2</sub>N<sub>2</sub> DMBE potential energy surface together with details of the computational method. The results are presented and discussed in Sections 3 and 4, correspondingly, while the major conclusions are gathered in Section 5.

## 2. Methodology

To represent the interatomic interaction, a global potential energy surface (PES) for the singlet ground electronic state of N<sub>2</sub>H<sub>2</sub> is used [16]. This function, depending upon the six interatomic distances, was constructed within the double many-body expansion [17] and calibrated to multireference configuration interaction *ab initio* energies [16,18]. Such a PES was previously used in dynamic studies of the NH + NH reaction [19] and the vibrational relaxation in nonreactive collisions of H<sub>2</sub> and N<sub>2</sub> [15]. For the interest of this work, from the N<sub>2</sub>H<sub>2</sub> DMBE PES, the reaction enthalpies are:



Although all the possible reactive channels were considered in the calculations (see later), only the above products were obtained in the energy interval covered in this study. Figure 1 shows a contour plot of the PES for the title reaction. Isoenergy lines identifying the output channels N<sub>2</sub>H + H and N<sub>2</sub> + H + H are also represented. Notice there are direct links between the reactants and the two product valleys here obtained, without passing through the four body moiety configuration region. This is also illustrated in Figure 2.

For molecular dynamic calculations, the quasiclassical trajectories method was used [20,21]. In trajectory calculations, we utilized an adapted version of the VENUS96 [22] code, coupled to the N<sub>2</sub>H<sub>2</sub> PES and making the appropriate assignment of all possible reactive channels (see Reference [19]). For the problems of interest, mentioned in the Introduction, the chosen relative diatom–diatom translational energy covered the range  $20.0 \leq E_{tr}/\text{kcal mol}^{-1} \leq 120.0$ ; while the selected initial vibrational quantum numbers for N<sub>2</sub> and H<sub>2</sub> were  $v' = 0, 4, 6, 8, 10, 12$  and  $v'' = 4, 6, 8, 10, 12$ , respectively. Figure 2 depicts a relaxed reaction path from the interaction potential together with the vibrational energy levels here considered. The corresponding energies for some combination of both reactants vibrationally excited were also included.

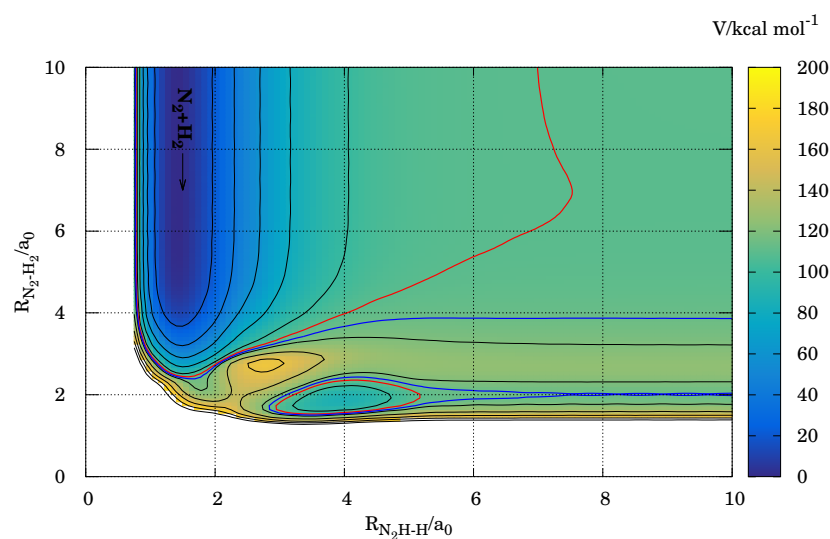


**Figure 1.** Contour plot of the DMBE  $N_2H_2$  PES for the  $N_2 + H_2$  reaction (black lines). The N–N bond distance, the NNH, and the NHH angles are partially relaxed. Red line contours stand for the  $N_2 + H + H$  dissociation limit, while blue line contours correspond to the  $N_2H + H$  channel.

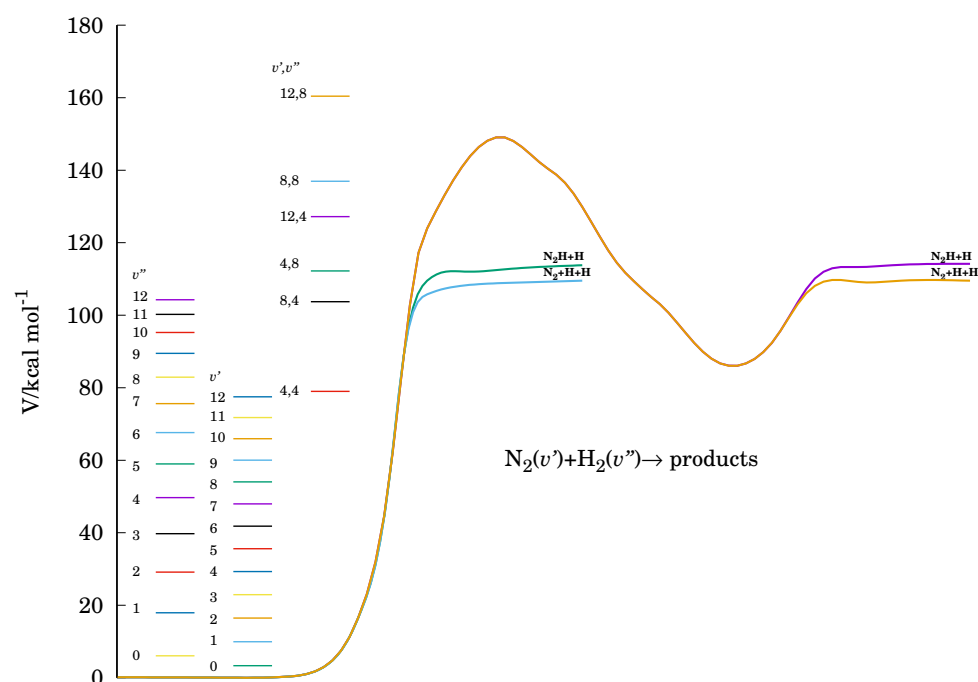


**Figure 2.** Energetics of a partially relaxed reaction path. Vibrational levels of the reactants and some combinations of both reactants vibrationally excited are also represented.

Additional calculations for translational energies in the interval  $140.0 \leq E_{tr}/\text{kcal mol}^{-1} \leq 200.0$  were also carried out for combinations  $v'' = 4, v' = 4$ ;  $v'' = 4, v' = 6$  and  $v'' = 5, v' = 4$  to improve the fitting of the excitation functions. Exploratory calculations were also carried with one or both reactants rotationally excited. Changes produced in the reaction probability due to the rotational effects are similar to the corresponding increase in translational energy. This subject will be addressed in future studies. Here, the initial rotational quantum numbers of the collision partners were fixed at the ground level  $j' = j'' = 0$  and are omitted heretofore.

The determination of the step size for numerical integration was performed by trial and error based on accuracy requirements. A value of  $1.0 \times 10^{-16}$  s was found to be sufficient to warrant the conservation of energy to more than 1 part in  $10^5$ . In turn, the

diatomic–diatomic initial separation was fixed at 15 Å, a value sufficiently large to make the interaction negligible. In turn, the maximum impact parameter  $b_{max}$ , which leads to the  $r$  reactive channel [23], was obtained following the usual procedure by computing batches of 800 trajectories for fixed values of  $b$  [15,19,24] and decreasing its value until a reactive trajectory was obtained. This procedure should allow for accuracy in  $b_{max}$  of about 0.1 Å; the calculated values are reported in Table 1. Batches of 10,000 trajectories were then carried out for each translational energy and vibrational combination. Such a number of trajectories were found to be enough to yield reactive cross-sections with an error of typically a few percent.

**Table 1.** Summary of the trajectory calculations for the reactive collisions  $H_2(v'') + N_2(v') \rightarrow N_2 + H + H$  within the IVEQMT approach.  $b_{max}$  in Å. Translational energies ( $E_{tr}$ ) are given in kcal mol<sup>-1</sup>. The symbol “-” indicates reactive channels remain closed.

$E_{tr}$	$v''$	$v'$	$b_{max}$	$N_T$	$N_r$	$v''$	$v'$	$b_{max}$	$N_T$	$N_r$
70.0	4	4	-	-	-	4	6	-	-	-
80.0			-	-	-			-	-	-
90.0			-	-	-			1.0	9996	27
100.0			1.1	9986	43			1.1	9984	76
110.0			1.1	9980	119			1.4	9982	128
120.0			1.4	9970	182			1.5	9980	249
70.0	4	8	-	-	-	4	10	-	-	-
80.0			-	-	-			0.5	9993	73
90.0			0.8	9986	74			1.1	9990	71
100.0			1.1	9985	110			1.1	9982	205
110.0			1.6	9977	131			1.6	9971	193
120.0			1.5	9971	314			1.5	9974	388
40.0	4	12	-	-	-	8	0	1.6	9846	182
50.0			-	-	-			2.0	9786	456
60.0			-	-	-			2.3	9944	710
70.0			0.4	9999	25			2.4	9674	890
80.0			0.7	9997	74			2.6	9664	937
90.0			1.1	9991	92			2.7	9660	1048
100.0			0.9	9976	363			2.5	9537	1387
110.0			1.4	9977	311			2.6	9509	1459
120.0			1.5	9973	453			2.6	9460	1616
30.0	8	4	-	-	-	8	6	0.6	10,000	7
50.0			2.2	10,000	412			2.2	10,000	405
60.0			2.3	9999	752			2.4	10,000	723
70.0			2.4	9999	952			2.5	9999	902
80.0			2.5	9998	1139			2.5	10,000	1163
90.0			2.5	9997	1330			2.6	9995	1258
100.0			2.6	9989	1436			2.6	9988	1469
110.0			2.7	9982	1572			2.6	9987	1726
120.0			2.6	9980	1830			2.6	9977	1946
30.0	8	8	0.6	10,000	13	8	10	1.1	10,000	12
50.0			2.2	10,000	429			2.1	10,000	488
60.0			2.4	10,000	711			2.4	10,000	716
70.0			2.5	10,000	929			2.5	10,000	936
80.0			2.5	9999	1167			2.5	10,000	1173
90.0			2.7	9998	1224			2.7	9997	1256
100.0			2.6	9996	1530			2.8	9998	1335
110.0			2.7	9988	1623			2.7	9991	1709
120.0			2.7	9975	1880			2.7	9989	1937

**Table 1.** *Cont.*

$E_{tr}$	$v''$	$v'$	$b_{max}$	$N_T$	$N_r$	$v''$	$v'$	$b_{max}$	$N_T$	$N_r$
10.0	8	12	-	-	-	12	0	2.8	9996	1297
20.0			-	-	-			3.4	9988	2381
30.0			0.5	10,000	26			3.5	9980	2925
40.0			-	-	-			3.6	9917	3093
50.0			2.0	10,000	540			3.5	9862	3487
60.0			2.5	10,000	684			3.6	9812	3388
70.0			2.5	10,000	945			3.6	9767	3477
80.0			2.5	10,000	1205			3.6	9712	3492
90.0			2.8	9998	1185			3.5	9675	3743
100.0			2.9	9995	1285			3.5	9684	3743
110.0			2.7	9992	1759			3.5	9640	3677
120.0			2.7	9997	1982			3.6	9696	3538
10.0	12	4	3.0	10,000	1164	12	6	3.0	9999	1169
30.0			3.6	9995	2798			3.6	9995	2813
50.0			3.6	9976	3405			3.6	9986	3411
80.0			3.6	9943	3680			3.6	9976	3706
100.0			3.7	9951	3607			3.7	9980	3632
120.0			3.6	9924	3747			3.6	9955	3785
10.0	12	8	2.9	9999	1255	12	10	3.0	9998	1213
30.0			3.6	9999	2867			3.7	9999	2722
50.0			3.7	9995	3286			3.6	9995	3467
80.0			3.4	9993	4184			3.5	9989	3958
110.0			3.5	9992	4051			3.5	9989	4086
120.0			3.6	9968	3800			3.6	9983	3854
10.0	12	12	3.1	10,000	1161					
30.0			3.6	10,000	2890					
50.0			3.6	9996	3452					
80.0			3.5	9994	3996					
110.0			3.6	9988	3869					
120.0			3.6	9993	3852					

The specific initial-state reactive cross-section for the channel  $r$  is calculated as:

$$\sigma_r(E_{tr}; v', v'') = \pi b_{max}^2 \frac{N_r}{N_T}, \quad (6)$$

with the corresponding uncertainties:

$$\Delta\sigma_r = \left( \frac{N_T - N_r}{N_T N_r} \right)^{\frac{1}{2}} \sigma_r \quad (7)$$

where  $N_r$  is the number of trajectories ending in the corresponding configurations for products  $r$  in a total  $N_T$ . For a given energetic combination of reactants, the reactive cross-section and the corresponding error for a specific output channel were calculated from relations (6) and (7). In this work, we adopted the following numerical criteria: when the obtained value of  $\sigma_r$  is smaller than seven times its corresponding error, the cross-section is negligibly small and the channel is considered as closed.

From the specific initial-state reactive cross-section and assuming a Maxwell–Boltzmann distribution over the translational energy  $E_{tr}$ , the specific initial-state reactive thermal rate coefficients are obtained as

$$k(T; v', v'') = g_e(T) \left( \frac{2}{k_B T} \right)^{3/2} \left( \frac{1}{\pi \mu} \right)^{1/2} \int E_{tr} \sigma_r(E_{tr}; v', v'') e^{-\frac{E_{tr}}{k_B T}} dE_{tr} \quad (8)$$

where  $k_B$  is the Boltzmann constant,  $\mu$  is the reduced mass of the colliding molecules,  $T$  is the temperature in kelvin, and  $g_e(T)$  the electronic degeneracy factor [25,26]. As the electronic states of  $N_2H_2$  and the collision partners are singlets,  $g_e$  assumes the value of 1.

Classical calculations permit molecular systems in configurations with the vibrational energy below their corresponding quantum minimal value or zero-point energy (ZPE). This ZPE leakage of the classical calculations can be eventually corrected after the trajectories integration. In this work, we selected the intermediate vibrational energy quantum mechanical threshold (IVEQMT) [27] to correct the ZPE problem. In the case of the IVEQMT approximation, trajectories ending in products with vibrational energy below a chosen fraction (here, 1/2) of the corresponding ZPE are considered as nonphysical and hence discarded [28]. As the number of rejected trajectories is relatively small, the calculation of new trajectories to replace them can be avoided [28].

### 3. Results

#### 3.1. Specific Initial-State Reactive Probability and Cross-Section

Table 1 summarized some trajectory results for selected initial states. Within the criteria used to define the closed channels, for the energy range covered in this study, the products formed were only  $N_2 + H + H$  (reaction (4)) and  $N_2H + H$  (reaction (5)). However, for the initial vibrational quantum number of  $H_2$  less than or equal to 3, both channels remained closed for all studied relative translational energies, independent of the vibrational energies of the  $N_2$ , while, in general, the reactive cross-section for  $N_2H + H$  formation was negligible. Thus, except when explicitly mentioned, the following discussion refers to reaction (4).

The calculated values of the specific initial-state reactive cross-section for the  $N_2 + H + H$  formation, according to the IVEQMT approach, are collected in Table 2, while Figure 3 shows the calculated points for the specific initial-state reactive cross-section for the  $N_2 + H + H$  formation vs. translational energy together with the associated error bars for the IVEQMT approximation.

In Figure 3, the vibrational excitation of the  $H_2$  molecule increases from Panel (a) to Panel (c) (showing examples of small, middle, and high vibrational excitation for the  $H_2$  molecule). Note that the threshold for the reaction (related to the translational energy) decreases and the excitation function increases with the vibrational energy of the  $H_2$  molecule (in our calculations, we considered the reactive channel open, when the initial-state reactive cross-section was, at least, 6 times greater than the calculated error). Note also that curves in Panel (a) of Figure 3 have values two orders lower than curves in Panel (c). This means that the level of the reactive cross-section depends on the  $H_2$  vibrational excitation.

**Table 2.** Specific initial-state cross-sections for reaction  $H_2(v'') + N_2(v') \rightarrow N_2 + H + H$  within the IVEQMT approach and the corresponding error, both in  $\text{\AA}^2$ . Translational energies ( $E_{tr}$ ) are given in  $\text{kcal mol}^{-1}$ .

$v''$	$v'$	$E_{tr}$	$\sigma$	$\Delta\sigma$	$v''$	$v'$	$E_{tr}$	$\sigma$	$\Delta\sigma$
4	4	90.0	-	-	4	6	90.0	0.0084	0.001
		100.0	0.0163	0.003			100.0	0.0289	0.233
		110.0	0.0452	0.004			110.0	0.0789	0.233
		120.0	0.1120	0.009			120.0	0.1763	0.011
4	8	80.0	-	-	4	10	80.0	0.0057	0.0006
		90.0	0.0148	0.001			90.0	0.0270	0.003
		100.0	0.0418	0.004			100.0	0.0780	0.005
		110.0	0.1056	0.009			110.0	0.1556	0.011
		120.0	0.2226	0.012			120.0	0.2749	0.013

Table 2. Cont.

$v''$	$v'$	$E_{tr}$	$\sigma$	$\Delta\sigma$	$v''$	$v'$	$E_{tr}$	$\sigma$	$\Delta\sigma$
4	12	40.0	-	-	8	0	40.0	0.1486	0.010
		50.0	-	-			50.0	0.5855	0.026
		60.0	-	-			60.0	1.1866	0.043
		70.0	0.0012	0.0002			70.0	1.6647	0.053
		80.0	0.0114	0.001			80.0	2.0591	0.063
		90.0	0.0350	0.003			90.0	2.4846	0.072
		100.0	0.0925	0.004			100.0	2.8555	0.070
		110.0	0.1920	0.011			110.0	3.2584	0.078
		120.0	0.3210	0.014			120.0	3.6278	0.082
8	4	50.0	0.6264	0.030	8	6	50.0	0.6158	0.029
		60.0	1.2500	0.044			60.0	1.3083	0.046
		70.0	1.7228	0.053			70.0	1.7712	0.056
		80.0	2.2368	0.062			80.0	2.2835	0.062
		90.0	2.6123	0.067			90.0	2.6729	0.070
		100.0	3.0530	0.074			100.0	3.1234	0.075
		110.0	3.6067	0.083			110.0	3.6703	0.080
120.0	3.8935	0.083	120.0	4.1422	0.084				
8	8	30.0	0.0014	0.0004	8	10	30.0	0.0045	0.001
		50.0	0.6523	0.030			50.0	0.6761	0.029
		60.0	1.2866	0.046			60.0	1.2956	0.046
		70.0	1.8240	0.057			70.0	1.8378	0.057
		80.0	2.2914	0.063			80.0	2.3031	0.063
		90.0	2.8037	0.075			90.0	2.8773	0.075
		100.0	3.2505	0.076			100.0	3.2881	0.082
		110.0	3.7214	0.084			110.0	3.9175	0.086
120.0	4.3164	0.089	120.0	4.4410	0.090				
8	12	10.0	-	-	12	0	10.0	3.1958	0.082
		20.0	-	-			20.0	8.6574	0.154
		30.0	0.0020	0.0004			30.0	11.2792	0.175
		40.0	-	-			40.0	12.6985	0.189
		50.0	0.6785	0.028			50.0	13.6073	0.185
		60.0	1.3430	0.049			60.0	14.0585	0.195
		70.0	1.8555	0.057			70.0	14.4943	0.197
		80.0	2.3660	0.064			80.0	14.6393	0.198
		90.0	2.9192	0.079			90.0	14.8886	0.190
		100.0	3.3957	0.087			100.0	14.8748	0.190
		110.0	4.0317	0.087			110.0	14.6792	0.190
120.0	4.5405	0.091	120.0	14.8566	0.199				
12	4	10.0	3.2911	0.090	12	6	10.0	3.3056	0.090
		30.0	11.3978	0.183			30.0	11.4588	0.183
		50.0	13.8968	0.193			50.0	13.9073	0.193
		80.0	15.0690	0.197			80.0	15.1252	0.196
		100.0	15.5895	0.207			100.0	15.6519	0.207
120.0	15.3727	0.198	120.0	15.4803	0.198				
12	8	10.0	3.31614	0.087	12	10	10.0	3.43036	0.092
		30.0	11.6741	0.184			30.0	11.7080	0.191
		50.0	14.1396	0.202			50.0	14.1229	0.193
		80.0	15.2055	0.179			80.0	15.2489	0.188
		110.0	15.6025	0.190			110.0	15.7420	0.189
120.0	15.5214	0.198	120.0	15.7183	0.198				
12	12	10.0	3.50514	0.096					
		30.0	11.7666	0.184					
		50.0	14.0604	0.193					
		80.0	15.3876	0.188					
		110.0	15.7715	0.198					
120.0	15.6944	0.198							

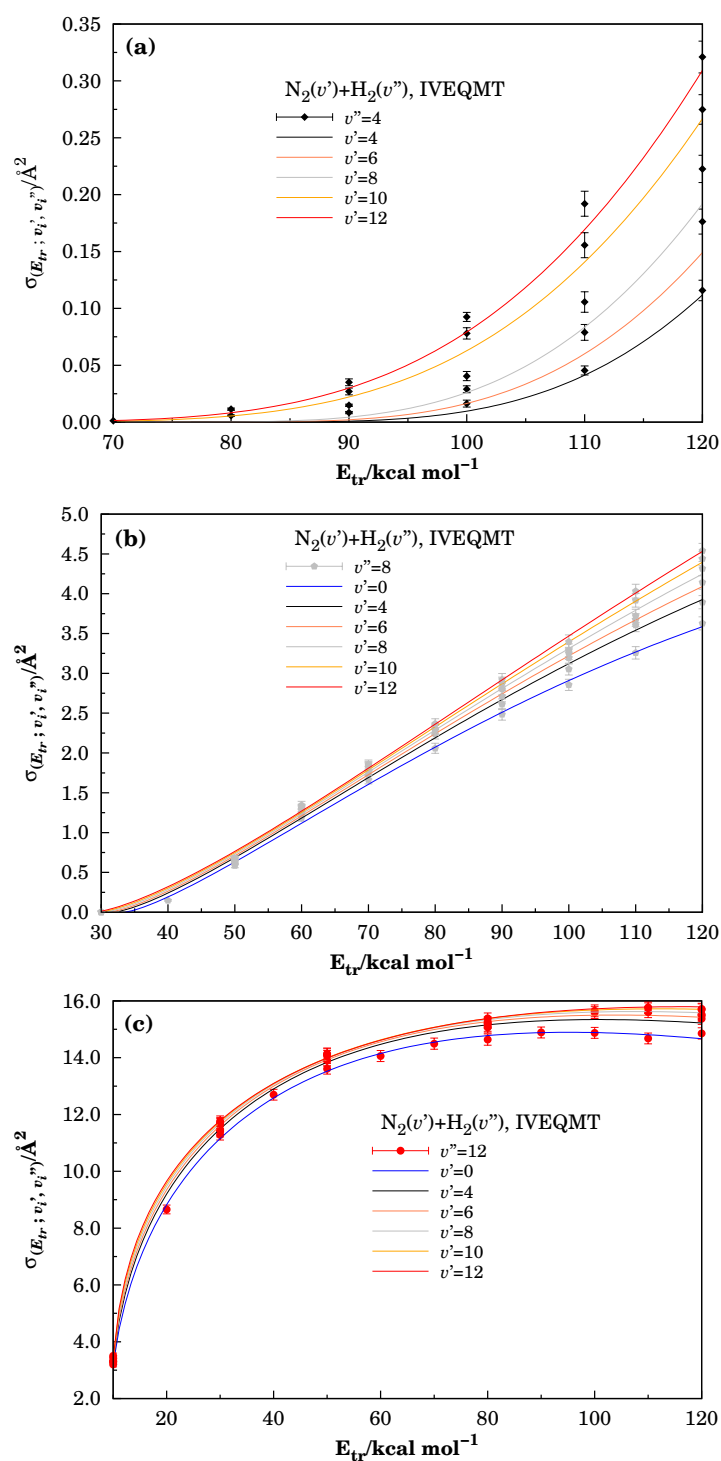


**Figure 3.** Specific initial-state reactive cross-section for the  $\text{N}_2 + \text{H} + \text{H}$  formation considering the reactive collisions  $\text{H}_2(v'') + \text{N}_2(v')$  inside the IVEQMT approach. In Panel (a)  $\text{H}_2(v'' = 4) + \text{N}_2(v' = 4, 6, 8, 10, 12)$ , in Panel (b)  $\text{H}_2(v'' = 8) + \text{N}_2(v' = 0, 4, 6, 8, 10, 12)$ , and in Panel (c)  $\text{H}_2(v'' = 12) + \text{N}_2(v' = 0, 4, 6, 8, 10, 12)$ .

For  $v'' \leq 3$ , the reactive channel remains closed (the threshold for  $\text{H}_2$  vibrational energy), inside the considered intervals for the translational energies and vibrational energies of the  $\text{N}_2$ . In the case of  $\text{H}_2(v'' = 4, 5)$ , the reaction channel (4) opens for the vibrational quantum numbers of the  $\text{N}_2$  that satisfy the conditions  $v' \geq 4$  (determining the total vibrational energy threshold for these cases). The described situation explains the small values of specific initial-state reactive cross-section reported in Panel (a), where

graphics corresponding to vibrational combinations near the mentioned vibrational energy threshold have been shown.

All panels in Figure 3 show that the vibrational excitation of the N<sub>2</sub> molecule leads to small increases in the initial-state reactive cross-section as expected from the great difference between the vibrational quanta of both molecules.

The analytical representation of the initial-state reactive excitation functions for vibrational levels included in Figure 3 follows the function [29]:

$$\sigma(E_{tr}; v', v'') = f_{E_{v''}, E_{v'}}(E_{tr} - E_{tr}^{E_{v''}, E_{v'}})^n \exp[-m^{E_{v''}, E_{v'}}(E_{tr} - E_{th}^{E_{v''}, E_{v'}})], \quad (9)$$

where the parameters  $f_{E_{v''}, E_{v'}}$ ,  $m^{E_{v''}, E_{v'}}$ ,  $n$ , and  $E_{th}^{E_{v''}, E_{v'}}$  were here expressed as the linear functions of the variable  $E_{v'}$

$$f_{E_{v''}, E_{v'}} = a_0 + a_1(E_{v'} - E_r) \quad (10)$$

$$m^{E_{v''}, E_{v'}} = b_0 + b_1(E_{v'} - E_r) \quad (11)$$

$$n = c_0 + c_1(E_{v'} - E_r) \quad (12)$$

$$E_{th}^{E_{v''}, E_{v'}} = d_0 + d_1(E_{v'} - E_r), \quad (13)$$

where  $E_r$  is the vibrational energy of the N<sub>2</sub> used as reference. For Panels (b) and (c), the reference is the energy of the level  $v' = 0$ , while in Panel (a), the fitting for the vibrational quantum numbers  $v' = 4, 6, 8$  takes as reference the energy for level  $v' = 4$  and for the case of vibrational quantum number  $v' = 10, 12$ , the energy reference corresponds to the level  $v' = 12$ .

The coefficients in the linear Equations (10)–(13) are reported in Table S1 of the Supplementary Material (SM). They vary with the vibrational energy of the H<sub>2</sub> molecule. We verified that the model works for all intermediate vibrational excitation of both molecules inside the intervals  $4 \leq v'' \leq 12$  and  $0 \leq v' \leq 12$ . Additional figures for the excitation functions of other vibrational combinations were included in the Figure S1 in the SM.

In all cases, the initial-state reactive cross-sections are increasing functions of initial translational and vibrational energies. For higher translational energies, the interactions between molecules during collisions are stronger because they could be closer, while the increase in the initial vibrational energies produces greater deformations of the excited molecule, leading to bigger collision areas and small increases in the quadrupole moment. The competition with other reactive channels produces in all cases the formation of a plateau. The onset of this behavior strongly depends on the vibration energy of the H<sub>2</sub>. While in Panel (c), it is observed after a translational energy of 60–70 kcal mol<sup>-1</sup> in Panels (a) and (b), it appears after 140–160 kcal mol<sup>-1</sup>. Despite the large values of the relative translational energies, the initial-state cross-sections for reaction have relatively small values, corresponding to the nonpolar character of both colliding molecules.

As mentioned in the first paragraph of this section, the reactive channel (5) is also opened with very small probabilities. To make a comparison with the reactive channel (4), the additional trajectories were calculated for H<sub>2</sub>( $v'' = 12$ ) + N<sub>2</sub>( $v' = 0$ ). The calculated specific initial-state reactive cross-sections are displayed in Figure S4 of the SM. These values are at least 40 times smaller than the corresponding for channel (4) for the same energetic initial conditions. Moreover, as was indicated in [19], the N<sub>2</sub>H molecule, as a rule, immediately produces N<sub>2</sub> + H + H; thus, it is possible to consider the reaction (5) as a slight contribution to the atomic hydrogen formation.

### 3.2. Energetic Features in the Reactive Molecular Ensemble

The discussion in the previous subsection points out the efficiency of the vibrational excitation of the H<sub>2</sub> molecule to produce the increase in reaction (4). In particular, it was demonstrated that for vibrational quantum numbers  $v'' \geq 6$  of the H<sub>2</sub>, the reaction (4) allows for translational energies greater than a determined value even when the N<sub>2</sub> is in

the ground vibrational state. Under the conditions of the present work, as was shown in Figures 1 and 2, reactive trajectories could also avoid the minimum of the PES and go directly to the products. Thus, calculations for these cases show that the barrier for the reaction (4) is determined by the energy difference between products and reactants in their ground electronic states. In all cases, the H<sub>2</sub> vibrational energy is essentially used to overpass that barrier and break the chemical bond.

Panel (a) of Figure 4 shows the arithmetic means of the energies corresponding to rotational degrees of freedom of the N<sub>2</sub> after reaction (4), while Panel (b) of the same figure reports the difference in the vibrational degrees of freedom of the N<sub>2</sub> in the products of the reaction (4) with their initial values. Finally, Panel (c) shows the difference between the arithmetic mean of the relative translational energy of the products and the value of the initial relative translational energy of reactants.

Panel (a) of Figure 4 shows an increase in the N<sub>2</sub> rotational energy mean value in the interval  $0.7 < E_{rot}^{N_2}/\text{kcal mol}^{-1} < 5.25$  with the increment of the relative translational energy. Such incremental results are practically independent of the vibrational energy of the molecule; thus, it is determined by the T-R processes. The observed slight increment in the rotational energy of the N<sub>2</sub> with the quantum number  $v'$  in the panel is probably due to the variation of inertial molecular properties when the molecular oscillations grow.

From the analysis of Panel (b) of Figure 4, with the exception of the N<sub>2</sub>( $v' = 0$ ) case (for which it is evident that it only has possibility to increase the vibrational energy), the figure shows a loss in the N<sub>2</sub> vibrational energy in the interval  $1.0 < E_{vib}^{N_2}/\text{kcal mol}^{-1} < 13.0$ . This energy loss is conditioned, principally, by the V-T processes but also includes a small transfer of energy used to break the chemical bond. This transferred energy warrants the small increase in the specific initial-state reactive cross-section with N<sub>2</sub> vibrational energy reported in Figure 3.

Following the previous analysis, one may rationalize that the energy associated with the relative translational degrees of freedom and the vibrational energy of the H<sub>2</sub> are the principal energy sources for the chemical reaction. To carry out an approximated quantitative energy balance, we introduced the following expression obtained from the energy conservation for the different processes discussed above:

$$E_{tr}^f - E_{tr}^i = (E_{vib,H_2}^i + E_{vib,N_2}^i - E_B) - E_{int,N_2}^f \quad (14)$$

where  $E_{tr}^i$  is the initial relative translational energy;  $E_{tr}^f$  is the arithmetic means of translational energies corresponding to the reactive molecular ensemble after the chemical reaction (4);  $E_{vib,H_2}^i$  and  $E_{vib,N_2}^i$  are the initial vibrational energies of the H<sub>2</sub> and N<sub>2</sub> molecules before reaction, respectively;  $E_B$  is the energy barrier for reaction (4) discussed above; and  $E_{int,N_2}^f$  is the arithmetic mean of the N<sub>2</sub> internal energy (the sum of vibrational and rotational energies) after reaction (of course, the arithmetic means were obtained from the trajectory calculations reported in the present work).

From Panel (c) of Figure 4, for the considered initial energy conditions, the molecular reactive ensemble experiences a significant cooling. To compare the results in Figure 4 with others obtained for different initial conditions, Figures S2 and S3 were included in the SM. In these figures, similar curves were reported for the initial conditions corresponding to collisions of H<sub>2</sub>( $v'' = 12$ ) + N<sub>2</sub>( $v' = 0, 6, 12$ ) (Figure S2) and H<sub>2</sub>( $v'' = 4$ ) + N<sub>2</sub>( $v' = 4, 6, 12$ ) (Figure S3). The curves in Figure S2 show that the N<sub>2</sub> experiences a small excitation when it is initially in its ground vibrational state, while in other situations it shows a loss of vibrational energy. In turn, the curves for the rotational degrees of freedom show a higher excitation than those observed in Figure 4 for H<sub>2</sub>( $v'' = 8$ ). On the other hand, the cooling process reported in the Panels (c) of both figures are less intensive in the case of Figure S2. Moreover, for the collisions H<sub>2</sub>( $v'' = 12$ ) + N<sub>2</sub>( $v' = 12$ ), the molecular reactive ensemble is slightly heated.

The comparison of Figure S3 with the other reported cases in Figures 4 and S2 leads to the conclusion that when the reactive processes diminish, the relaxation processes are

more relevant, leading to the highest rotational excitation, a stronger loss of  $N_2$  vibrational energy, and, in general, the heating of the molecular reactive ensemble.

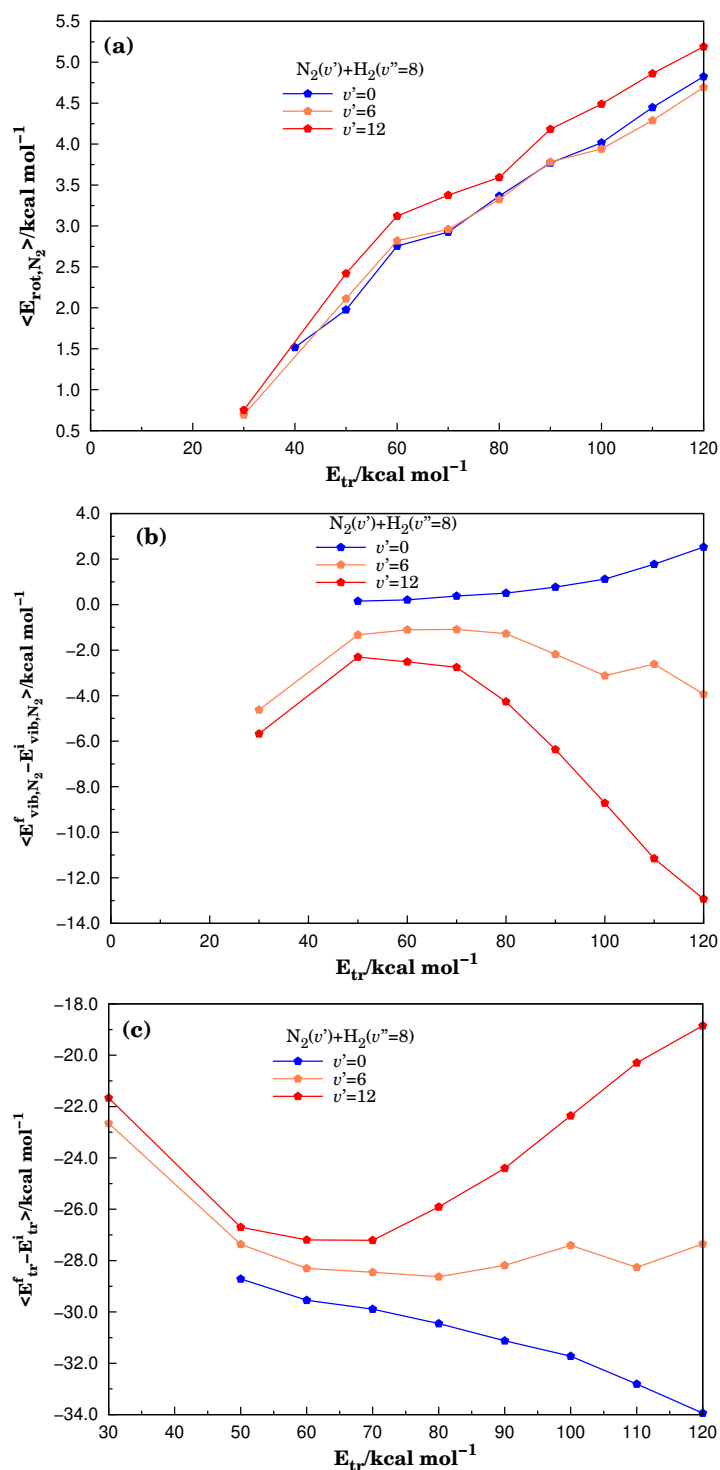


**Figure 4.** Comparison of the arithmetic mean of energies for different degrees of freedom in the reaction (4) within the IVEQMT approach versus translational energies when the reactants are the  $H_2(v'' = 8)$  and the  $N_2$  in the vibrational excited states  $v' = 0, v' = 6, v' = 12$ . In Panel (a), the mean values of the rotational energy for the product  $N_2$  are displayed. In Panel (b), the differences between the mean values of the vibrational energy for the  $N_2$  after reaction and the corresponding initial value are shown. In Panel (c), the differences between mean values of the relative translational energy of the molecular system after reaction and the corresponding initial values are presented.

### 3.3. Specific Initial-State Reactive Thermal Rate Coefficients

From the specific initial-state reactive cross-sections Equation (9) and using the integral in Equation (8), one then obtains:

$$k(T; v', v'') = \left( \frac{8k_B T}{\pi \mu} \right)^{1/2} f_{E_{v'', E_{v'}}}(k_B T)^n \exp\left( \frac{-E_{v'', E_{v'}}}{k_B T} \right) \left[ \Gamma(n+2) \left( m^{E_{v'', E_{v'}}} k_B T + 1 \right)^{-(n+2)} + \frac{E_{v'', E_{v'}}}{k_B T} \Gamma(n+1) \left( m^{E_{v'', E_{v'}}} k_B T + 1 \right)^{-(n+1)} \right] \quad (15)$$

for the specific initial-state reactive thermal rate coefficients as a function of the temperature. Here,  $\Gamma(\dots)$  is the gamma function.

Figure 5 shows the curves of the specific initial-state reactive thermal rate coefficients for the same combinations of vibrational energies used before for the calculations of the corresponding cross-sections within the approaches IVEQMT. As expected from the specific initial-state cross-sections, they are increasing the functions of both vibrational and relative translational energies, and for a fixed vibrational excitation of the H<sub>2</sub>, the increase in the N<sub>2</sub> vibrational energy produces only slight growths in the specific initial-state thermal rate coefficients.

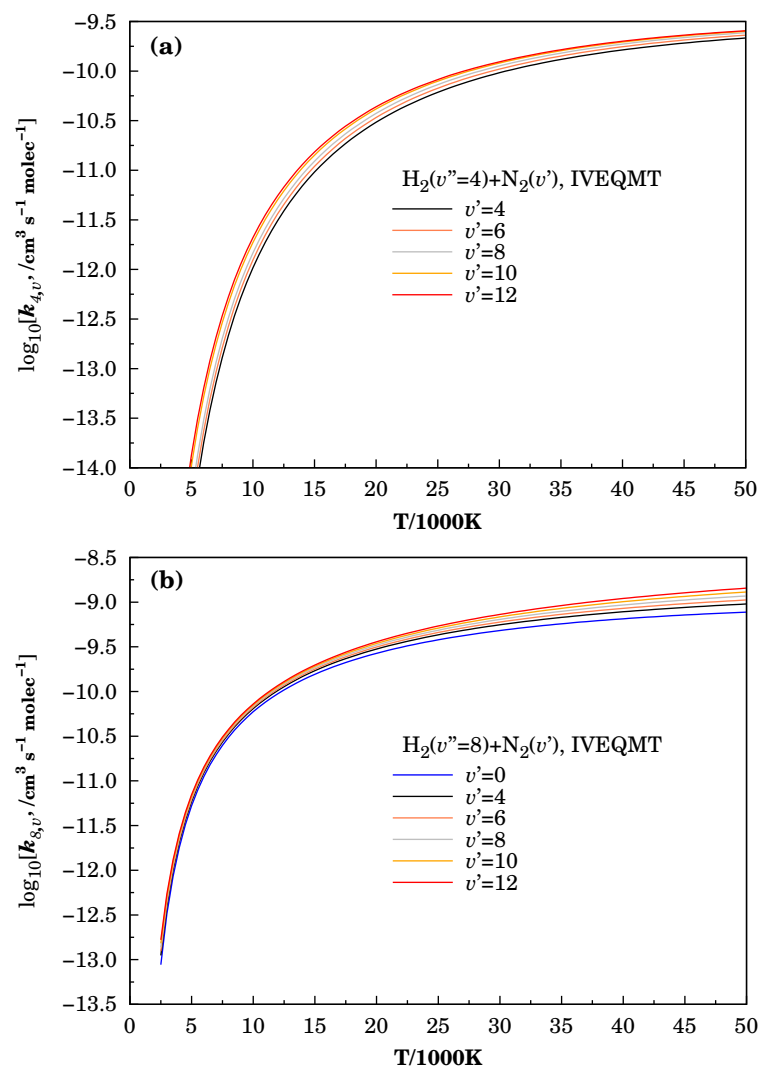
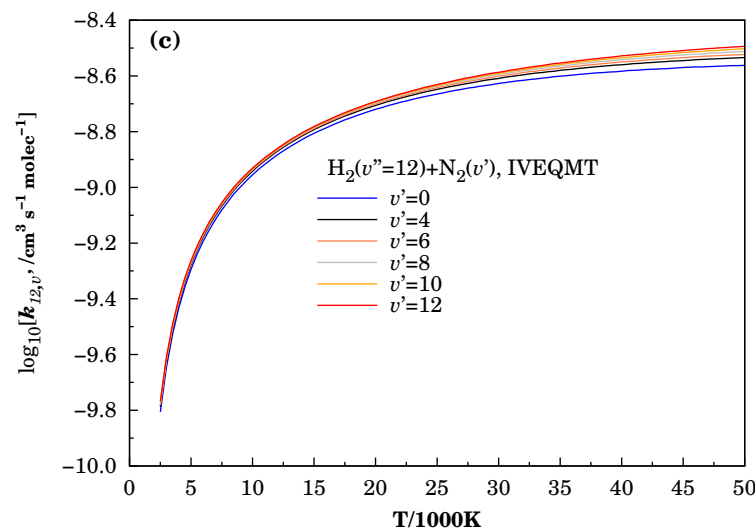


Figure 5. Cont.



**Figure 5.** Specific initial-state reactive thermal rate coefficients for the  $\text{N}_2 + \text{H} + \text{H}$  formation considering the reactive collisions  $\text{H}_2(v'') + \text{N}_2(v')$  inside the IVEQMT approach. In Panel (a)  $\text{H}_2(v'' = 4)$ , in Panel (b)  $\text{H}_2(v'' = 8)$ , and in Panel (c)  $\text{H}_2(v'' = 12)$ .

#### 4. Discussion

The analysis conducted in the subsection “Energetic Features in the Reactive Molecular Ensemble” points out that the majority of the initial energy combinations leading to reaction produce a decrease in the translational energy; thus, considering the values of the vibrational average thermal rate coefficients for the reaction (4) here reported, it could be necessary to account for this decrease in the translational energy to calculate the temperature of the gas behind the shock wave in the modeling works devoted to the hypersonic flights.

Figure 6 shows the vibrational average thermal rate coefficients for different situations. The red curves in this figure corresponds to the vibrational average thermal rate coefficients for reaction (4) calculated using the equation

$$\langle k(T; v', v'') \rangle = \frac{\left\{ \sum_{v'_i} \sum_{v''_i} \omega_{v'_i} \omega_{v''_i} [k(T; v', v'')] \right\}}{\sum_{v'_i} \sum_{v''_i} \omega_{v'_i} \omega_{v''_i}}, \quad (16)$$

where  $\omega_{v'_i}$  and  $\omega_{v''_i}$  are the vibrational populations of  $\text{N}_2$  and  $\text{H}_2$ , respectively, while the blue curves represent the vibrational average thermal rate coefficients  $2 \times \langle k(T; v', v'') \rangle$  that determine the temporal variation of the H concentration following the equation:

$$\frac{d[\text{H}]}{dt} = 2 \times \langle k(T; v', v'') \rangle [\text{H}_2][\text{N}_2]. \quad (17)$$

Both curves experience a very rapid increase until the formation of a high-value plateau after the translational temperature of 15,000 K. Such temperatures, and higher, are obtained in the modeling studies reported in [1–3] for the shock wave produced by hypersonic objects in the atmosphere; thus, the formation of abundant atomic hydrogen considering the high chemical rate predicted by Equation (17) is a real possibility in the air around hypersonic objects.

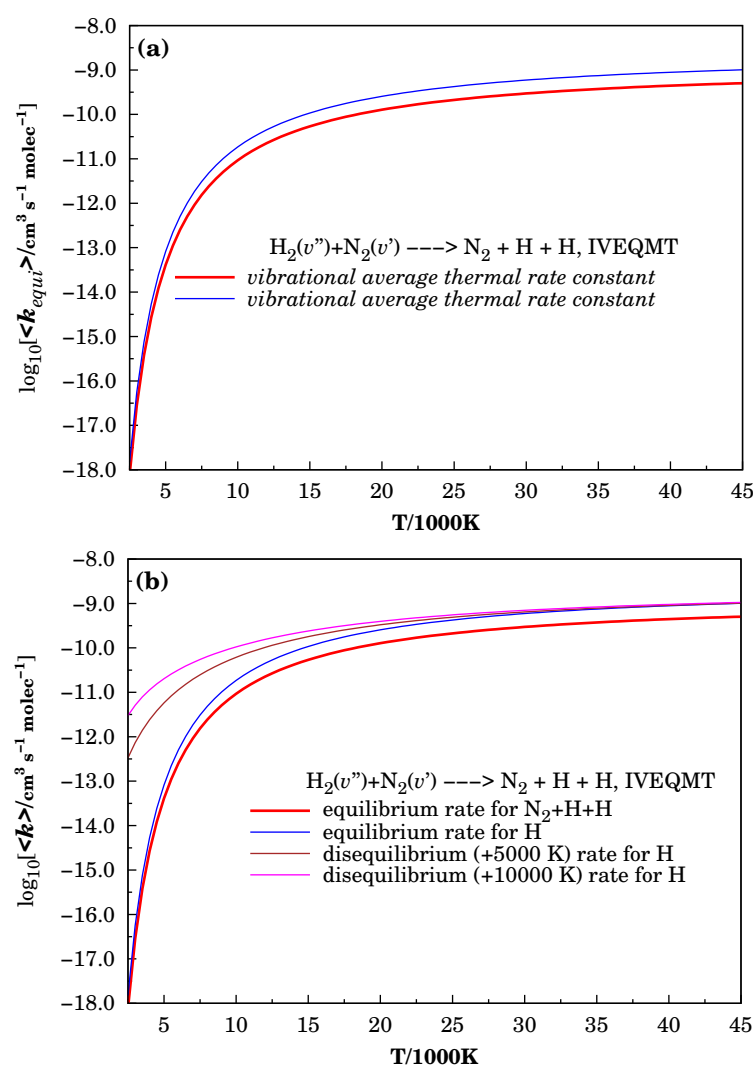


**Figure 6.** Calculated vibrational average thermal rate coefficients for studied processes. In Panel (a) for the  $\text{N}_2 + \text{H} + \text{H}$  formation (red curve) and atomic hydrogen formation (blue curve) considering a Boltzmann distribution for the population of vibrationally excited reactants at the calculated temperature. In Panel (b), together with the curves previously described in Panel (a), the vibrational average thermal rate coefficients for atomic hydrogen formation considering thermal disequilibrium conditions for the vibrational populations of reactants are shown (see text for description).

In a recent paper [30], a QCT study of the reaction (18) for a wide range of temperatures ( $300 \leq T/\text{K} \leq 20,000$ ) was presented. The total rate for the reaction (18) was reported, including also the weighted contribution of the



$^2\text{A}'$  and  $^4\text{A}'$  surfaces. Independently of the quantitative differences which are expected for different systems, the qualitative similarities between the rate constants are remarkable.

As expected, from the rapid expansion of the gas behind the shock wave, high thermal nonequilibrium conditions in the gas layer near the moving objects are reported in the mentioned papers [1–3]. To make a qualitative evaluation of the effect of the disequilibrium conditions on the atomic hydrogen formation, the curves calculated considering the hypothetical hot Boltzmann distribution shifted in 5000 K (brown curve) and 10,000 K (magenta curve) are represented in Panel (b) of the Figure 6. These curves show that, under nonequilibrium conditions, their plateau behavior is retained until the translational temperature around 10,000 K, and the values of the average thermal rate coefficients for

temperatures below 7500 K are, at least, one order of magnitude higher than those obtained under thermal equilibrium conditions. Considering the high values of the average thermal rate coefficients in Equation (16), it is possible to expect the conversion of a considerable quantity of molecular hydrogen in atomic hydrogen that could enter important atmospheric reactions as (1)–(3), leading to a relatively significant atmospheric impact. Finally, we should mention that no comparison with experimental data was possible since, to our knowledge, no such data exist in the literature for the interval of temperature considered in the present work.

## 5. Conclusions

In this work, we have reported a quasiclassical dynamic study of the  $N_2(v') + H_2(v'')$  reaction for several vibrational states of the reactants ( $0 \leq v' \leq 12; 0 \leq v'' \leq 12$ ) and a wide range of relative translational energy ( $20 \leq E_{tr} / \text{kcal mol}^{-1} \leq 120$ ). According to our calculation, the most probable product was  $N_2 + H + H$ . The formation of  $N_2H$  was also observed, with a negligible contribution to total reaction. As expected, the vibrational energy in the  $H_2$  molecule has a determinant role in the dissociation process. The initial vibrational energy content in  $N_2$  is partially used in dissociating the molecular hydrogen. The reaction excitation functions exhibit typical shapes for barrier-like processes, and the models were correspondingly presented. Specific initial-state thermal rate coefficients reaction and vibrationally averaged rate constants were reported. The relatively high values of these rates for the considered conditions indicate the role of the title reaction in atmospheric issues involving high temperatures might be important, particularly as a source of atomic hydrogen. Of course, such a verification requires considering the reaction in the kinetic models. The energetic analysis of the calculated trajectories points toward a cooling effect when transforming the molecular hydrogen in the dissociated form by collisions with vibrationally excited molecular nitrogen.

**Supplementary Materials:** The following are available at <https://www.mdpi.com/article/10.3390/atmos12101349/s1>, Table S1, Figures S1–S4.

**Author Contributions:** Conceptualization, J.d.D.G. and M.Y.B.; data curation, J.d.D.G.; writing—review and editing, J.d.D.G. and M.Y.B. All authors have read and agreed to the published version of the manuscript.

**Funding:** This research was funded by Conselho Nacional de Desenvolvimento Científico e Tecnológico (CNPq).

**Data Availability Statement:** The data presented in this study are available alongside the article and the Supplementary Material.

**Conflicts of Interest:** The authors declare no conflict of interest.

## Abbreviations

The following abbreviations are used in this manuscript:

PES	Potential Energy Surface
QCT	Quasiclassical Trajectories
IVEQMT	Intermediate Vibrational Energy Quantum Mechanical Threshold
ZPE	Zero-Point Energy
V-T processes	Energy transfer from vibrational to translational degrees of freedom
T-R processes	Energy transfer from translational to rotational degrees of freedom

## References

1. Keidar, M.; Kim, M.; Boyd, I.D. Electromagnetic Reduction of Plasma Density During Atmospheric Reentry and Hypersonic Flights. *J. Spacecr. Rocket.* **2008**, *45*, 445. [CrossRef]
2. Josyula, E.; Suchyta, C.J.; Vedula, P.; Burt, J.M. Multiquantum Transitions in Oxygen and Nitrogen Molecules in Hypersonic Non-equilibrium Flows. *J. Thermophys. Heat Transf.* **2019**, *33*, 378–391. [CrossRef]

3. Shoev, G.; Oblapenko, G.; Kunova, O.; Mekhonoshina, M.; Kustova, E. Validation of vibration-dissociation coupling models in hypersonic non-equilibrium separated flows. *Acta Astronaut.* **2018**, *144*, 147–159. [[CrossRef](#)]
4. Koner, D.; Bemish, R.J.; Meuwly, M. Dynamics on Multiple Potential Energy Surfaces: Quantitative Studies of Elementary Processes Relevant to Hypersonics. *J. Phys. Chem. A* **2020**, *124*, 6255–6269. [[CrossRef](#)] [[PubMed](#)]
5. Josyula, E. Oxygen Atoms' Effect on Vibrational Relaxation of Nitrogen in Blunt-Body Flows. *J. Thermophys. Heat Trans.* **2001**, *15*, 106–115. [[CrossRef](#)]
6. Kustova, E.V.; Oblapenko, G.P. Reaction and internal energy relaxation rates in viscous thermochemically non-equilibrium gas flows. *Phys. Fluids* **2015**, *27*, 016102, [[CrossRef](#)]
7. Kustova, E.V.; Oblapenko, G.P. Mutual effect of vibrational relaxation and chemical reactions in viscous multitemperature flows. *Phys. Rev. E* **2016**, *93*, 033127. [[CrossRef](#)] [[PubMed](#)]
8. Wayne, R.P. *Chemistry of Atmospheres*; Oxford University Press: Oxford, UK, 2002.
9. Jacob, D.J. *Introduction to Atmospheric Chemistry*; Princeton University Press: Princeton, NJ, USA, 1999.
10. Mackenzie, F.; Mackenzie, J.A. *Our Changing Planet*; Prentice-Hall: Upper Saddle River, NJ, USA, 1995.
11. Atkinson, R.; Baulch, D.L.; Cox, R.A.; Hampson, J.R.F.; Troe, J.A. Evaluated kinetic and photochemical data for atmospheric chemistry. Supplement III. *J. Phys. Chem. Ref. Data* **1989**, *18*, 881. [[CrossRef](#)]
12. Atkinson, R.; Baulch, D.L.; Cox, R.A.; Hampson, R.F., Jr.; Kerr, J.A.; Rossi, M.J.; Troe, J. Evaluated kinetic, photochemical and heterogeneous data for atmospheric chemistry: Supplement V. IUPAC Subcommittee on Gas Kinetic Data Evaluation for Atmospheric Chemistry. *J. Phys. Chem. Ref. Data* **1997**, *26*, 521–1011. [[CrossRef](#)]
13. Gordiets, B.; Ferreira, C.; Pinheiro, M.; Ricard, A. Self-consistent kinetic model of low-pressure N<sub>2</sub>-H<sub>2</sub> flowing discharges: I. Volume processes. *Plasma Sources Sci. Technol.* **1998**, *7*, 363–378. [[CrossRef](#)]
14. Gordiets, B.; Ferreira, C.M.; Pinheiro, M.J.; Ricard, A. Self-consistent kinetic model of low-pressure N<sub>2</sub>-H<sub>2</sub> flowing discharges: II Surface processes and densities of N, H, NH<sub>3</sub> species. *Plasma Sources Sci. Technol.* **1998**, *7*, 379–388. [[CrossRef](#)]
15. de Dios Garrido, J.; Ballester, M.Y. Relaxation processes in non-reactive collisions of H<sub>2</sub> and N<sub>2</sub> at high translational energies. *Mol. Phys.* **2021**, *119*, e1831635, [[CrossRef](#)]
16. Poveda, L.A.; Biczysko, M.; Varandas, A.J.C. Accurate ab initio based DMBE potential energy surface for the ground electronic state of N<sub>2</sub>H<sub>2</sub>. *J. Chem. Phys.* **2009**, *131*, 044309. [[CrossRef](#)]
17. Varandas, A.J.C. Intermolecular and Intramolecular Potentials: Topographical Aspects, Calculation, and Functional Representation via A Double Many-Body Expansion Method. In *Advances in Chemical Physics*; John Wiley & Sons, Ltd.: Hoboken, NJ, USA, 2007; Chapter 2, pp. 255–338. [[CrossRef](#)]
18. Biczysko, M.; Poveda, L.; Varandas, A. Accurate MRCI Study of Ground-State N<sub>2</sub>H<sub>2</sub> Potential Energy Surface. *Chem. Phys. Lett.* **2006**, *424*, 46–53. [[CrossRef](#)]
19. de Castro, D.G.; Poveda, L.A.; Crispim, L.W.S.; Ballester, M.Y. Quasi-Classical Trajectory Study of NH(<sup>3</sup>Σ<sup>-</sup>) + NH(<sup>3</sup>Σ<sup>-</sup>) Reactive Collisions. *J. Phys. Chem. A* **2019**, *123*, 9113–9122. [[CrossRef](#)] [[PubMed](#)]
20. Karplus, M.; Porter, R.N.; Sharma, R.D. Exchange Reactions with Activation Energy. I. Simple Barrier Potential for (H, H<sub>2</sub>). *J. Chem. Phys.* **1965**, *43*, 3259–3287. [[CrossRef](#)]
21. Karplus, M.; Porter, R.N.; Sharma, R.D. Dynamics of reactive collisions: The H + H<sub>2</sub> exchange reaction. *J. Chem. Phys.* **1964**, *40*, 2033–2034. [[CrossRef](#)]
22. Hase, W.L.; Duchovic, R.J.; Hu, X.; Komornik, A.; Lim, K.F.; Lu, D.H.; Peslherbe, G.H.; Swamy, K.N.; van de Linde, S.R.; Varandas, A.J.C.; et al. VENUS 96. *Quantum Chem. Program Exch. Bull.* **1996**, *16*, 43.
23. Levine, R.D. *Molecular Reaction Dynamics*; Cambridge University Press: Cambridge, UK, 1995.
24. Garrido, J.d.D.; Ellakkis, S.; Ballester, M.Y. Relaxation of Vibrationally Excited OH Radical by SO. *J. Phys. Chem. A* **2019**, *123*, 8994–9007. [[CrossRef](#)]
25. Truhlar, D.G. Multiple Potential Energy Surfaces for Reactions of Species in Degenerate Electronic States. *J. Chem. Phys.* **1972**, *56*, 3189–3190. [[CrossRef](#)]
26. Muckerman, J.T.; Newton, M.D. Comment on “Multiple Potential Energy Surfaces for Reactions of Species in Degenerate Electronic States” by D. G. Truhlar. *J. Chem. Phys.* **1972**, *56*, 3191–3192. [[CrossRef](#)]
27. Varandas, A.J.C. Excitation function for H + O<sub>2</sub>: A study of zero-point energy effects and rotational distributions in trajectory calculations. *J. Chem. Phys.* **1993**, *99*, 1076. [[CrossRef](#)]
28. Varandas, A.J.C. A novel nonactive model to account for the leak of zero-point energy in trajectory calculations. Application to H + O<sub>2</sub> reaction near threshold. *Chem. Phys. Lett.* **1994**, *225*, 18. [[CrossRef](#)]
29. LeRoy, R.L. Relationships between Arrhenius activation energies and excitation functions. *J. Phys. Chem.* **1969**, *73*, 4338. [[CrossRef](#)]
30. Veliz, J.C.S.V.; Koner, D.; Schwilk, M.; Bemish, R.J.; Meuwly, M. The N(<sup>4</sup>S) + O<sub>2</sub>(X<sup>3</sup>Σ<sub>g</sub><sup>-</sup>) → O(<sup>3</sup>P) + NO(X<sup>2</sup>Π) reaction: thermal and vibrational relaxation rates for the <sup>2</sup>A', <sup>4</sup>A' and <sup>2</sup>A'' states. *Phys. Chem. Chem. Phys.* **2020**, *22*, 3927. [[CrossRef](#)] [[PubMed](#)]